Applied Catalysis B: Environmental 314 (2022) 121476

Contents lists available at ScienceDirect

Applied Catalysis B: Environmental

journal homepage: www.elsevier.com/locate/apcatb

Unveiling the origin of alkali metal promotion in CO_2 methanation over Ru/ZrO_2

Mengting Gao [a,b,1], Jin Zhang [a,b,1], Pengqi Zhu [a], Xingchen Liu [a,*], Zhanfeng Zheng [a,b,**]

[a] State Key Laboratory of Coal Conversion, Institute of Coal Chemistry, Chinese Academy of Sciences, Taiyuan 030001, China
[b] Center of Materials Science and Optoelectronics Engineering, University of Chinese Academy of Sciences, Beijing 100049, China

ARTICLE INFO

Keywords:
Alkali metal promoters
Ru/ZrO_2
CO_2 methanation
Dissociation of CO*
Electron back-donation

ABSTRACT

Alkali metals are used as promoters in a broad range of catalytic reactions involving supported metal catalysts, and the origin of their promotional effects has become one of the fundamental questions in heterogeneous catalysis. However, a thorough understanding of the promotional mechanism is still unclear. Combining experiments and theory, the effects of alkali metals on the reactivity of CO_2 methanation reaction over Ru/ZrO_2, a crucial reaction for CO_2 utilization is explored. The conventionally assumed electron enrichment of Ru is not the decisive factor for the promotion. Rather, Na promotion facilitate the adsorption and dissociation of CO on the local interfacial Ru sites of Ru/ZrO_2, which is the key step of CO_2 methanation process. The feasible dissociation of CO on the alkali metal promoted Ru/ZrO_2 originates from the enhanced electron back-donation from the interfacial Ru sites, which leads to more than an order of magnitude increase in CO_2 conversion activity.

1. Introduction

Catalytic hydrogenation of CO_2 into value-added hydrocarbons using hydrogen from renewable sources is highly desirable in combating the environment and energy crisis. Among them, power to gas (PtG) concept has drawn much attention, where H_2 generated from renewable energy is converted into CH_4 as an alternative resource of natural gas [1,2]. This technology, which was proposed firstly in 1902 by Sabatier, is gaining new currency again recently due to the surging demand of mitigating the climate change and tackling the energy depletion crisis [3]. Despite much efforts have been paid, this process still suffers from low activity and stability at mild conditions [4]. The complexity of the reaction also hinders the exploration of more efficient catalysts. Therefore, it is crucial to explore effective methods to optimize the complex process.

Since the first report about the promotional effects of alkali metals in heterogeneous catalysis in 1845 [5], the catalytic effect of alkali metals has been studied widely in various hydrogenation reactions [6–8]. It has been proposed that modification of alkali metal over metal catalysts often works as electron donor in modifying their electron structure and improving the hydrogenation reactivity. Thus the adsorption ability of metal center towards the reactants and intermediates could be affected by the electron rich effect introduced by the alkali metal promoters [9]. Others hold the points that alkali metals interact with the metal centers by the oxygen atoms between them. Such an interaction can improve the stability of the catalysts by preventing the sintering of active metals, which may play an indirect role in the modification of active metal centers [10].

It is intriguing that the addition of alkali metals has variable effects in the CO_2 hydrogenation process. Heyl et al. reported that the adsorption strength of CO and the dissociation ability of H_2 are both affected by alkali metal addition on Rh/Al_2O_3. As a result, the desorption of CO is favored and the methanation of CO is suppressed [11]. According to An et al., CO_2 activation was accelerated in the presence of K on Cu_xO/Cu (111) owing to the geometric and electronic effects introduced by K [12]. In contrast, the electrochemical promotion of Na^+ conducting support on CO_2 methanation was also reported on Ru porous catalyst films [13], which was attributed to the suppressed desorption of CO by the increasing potential for its production. Paraskevi reported that the population of CO species on Ru increases with the presence of alkali metals. The activity and selectivity toward methane both increase with the addition of alkali metals. [14]. Despite the previous reports on the effects of alkali metals in hydrogenation of CO_2, no consistent

* Corresponding author.
** Corresponding author at: State Key Laboratory of Coal Conversion, Institute of Coal Chemistry, Chinese Academy of Sciences, Taiyuan 030001, China.
E-mail addresses: liuxingchen@sxicc.ac.cn (X. Liu), zfzheng@sxicc.ac.cn (Z. Zheng).
[1] These authors contributed equally to this work.

https://doi.org/10.1016/j.apcatb.2022.121476
Received 29 January 2022; Received in revised form 21 April 2022; Accepted 3 May 2022
Available online 5 May 2022

agreements have been reached. The exact role of alkali metal in CO_2 hydrogenation on supported metal catalyst is still ambiguous.

Among the group VIII metals with high methanation activity, Ru was proven to be the most active methantion catalyst [15]. In addition, ZrO_2 has excellent adsorption capacity for CO_2 [16], which was recognize as a potential carrier for CO_2 hydrogenation reactions. Therefore, ZrO_2 supported subnanometric Ru shows excellent performances in CO_2 methanation [17]. Here, take Ru/ZrO_2 as an example, the effects of alkali metals on the hydrogenation of CO_2 on supported catalyst are explored in details. By probing the CO_2 hydrogenation process over alkali metal modified Ru/M-ZrO_2 (M=Li, Na, and K), the promotional effects of alkali metals on the electronic structure and evolution of intermediates were revealed by experimental and theoretical measurements. The explorations provide atomic level insights into how the alkali metals modulate the catalytic performance of Ru/ZrO_2 in CO_2 conversion, and pave new avenues to the engineering of supported metal catalysts with alkali metal promoters.

2. Experimental section

2.1. Preparation of Ru/ZrO_2 and Ru/M-ZrO_2 (M=Li, Na and K)

ZrO_2 was prepared by precipitation method [18]. Typically, $ZrCl_4$ was dissolved into 60 mL ultrapure water (0.16 mol/L) under stirring followed by adding ammonia solution dropwise to adjust the pH value of 10. The solution was heated to 50 °C and kept on stirring vigorously for 24 h. Then the suspension was filtered and washed with ultrapure water to reach the pH= 7. The product was collected and dried under vacuum at 60 °C over night. Finally, ZrO_2 was obtained by calcining the solid under flowing air at 400 °C (heating rate of 5 °C/min) for 4 h.

Ru/ZrO_2 and alkali metal promoted Ru/M-ZrO_2 (M=Li, Na and K) were prepared by wet impregnation method [19]. The alkali metal modified ZrO_2 was prepared by impregnating 1 g prepared ZrO_2 powder into 50 mL aqueous solution containing the appropriate amount of $LiNO_3$ (30 mg), Na_2CO_3 (23 mg), or K_2CO_3 (30 mg), respectively, which corresponding to the equal nominal moles of alkali metal elements (4.35×10^{-4} mol). The according nominal mass fraction of alkali metals relative to ZrO_2 is 0.30 wt%, 1.00 wt%, and 1.70 wt%, respectively. The resulting solution was stirred at 50 °C for 2 h and maintained at 80 °C until the water was evaporated. Then alkali metal promoted ZrO_2 was obtained after dried at 60 °C over night and calcinated in air at 400 °C (heating rate of 5 °C/min) for 4 h. Ru supported ZrO_2 was obtained by impregnating the prepared ZrO_2 or alkali metal promoted ZrO_2 with $RuCl_3$ solution by the same impregnation procedure. Exceptionally, the sample was calcined under flowing H_2 (50 mL/min) at 200 °C (heating rate of 10 °C /min) for 2 h.

2.2. Characterization

Power X-ray diffraction (XPD) was performed by a MiniFlex II diffractometer using Cu Kα radiation (λ = 1.54 Å) operating in the 2θ range of 10–80°. High-resolution transmission electron microscopy (HRTEM) images and energy dispersive X-ray (EDX) mapping was record on a JEM-2010 instrument at 200 kV. The content of Ru and alkali metals was measured by inductively coupled plasma atomic emission spectroscopy (ICP-OES) by Thermo iCAP6300 spectrometer. The valence states of the sample were analyzed by X-ray photoelectric spectroscopy (XPS) using USA Thermo ESCALAB 250 (Al Kα source, hν=1486 eV). The spectras were calibrated to the C 1 s position of 284.86 eV and analyzed by XPSPEAK41 software. CO temperature-programmed desorption (CO-TPD) and CO chemisorption were performed by a Micromeritics BELCAT-B apparatus using 50 mg catalyst. In the measurements, the catalyst was pretreated with H_2 under 300 °C for 1 h and purge with Ar for 30 min. After the temperature was reduced to 50 °C, CO was introduced for 1 h. Ar was used to remove the physical absorbed CO for 30 min. Then the spectra was cllected by heating the sample from 50 °C to 700 °C at the heating rate of 10 °C/min. In CO chemisorption measurement, after the sample was cooled down to 50 °C, CO (5%CO in He) was introduced repeatedly until saturated adsorption of CO was reached. The dispersion of Ru was calculated by assuming that the adsorption stoichiometry of CO and Ru was 2:1.

2.3. In-situ DFRIFTS studies

According to the previous analysis procedure of CO_2 methanation [20], the interaction between H_2/CO_2 (3:1 in volume) mixture and the catalysts was performed by in-situ diffuse reflectance infrared Fourier transform spectroscopy (DRIFTS) using Bruker Tensor II spectrometer equipped with the mercury cadmium telluride detector cooled down by liquid nitrogen. Before test, the catalyst was prereduced under H_2 (50 mL/min) at 200 °C for 2 h. After that, the catalyst was placed into the sample holder followed by heated and maintained at 200 °C under highly purity Ar (25 mL/min) for 2 h. Then the background scan was record. Finally, the flow was switched to CO_2/H_2 mixture (1%CO_2 +3% H_2 in Ar) for 15 min and the differential spectra was collected for 1 h with 1 min interval. The measurements of CO adsorption were performed by the same procedure except for the flowing was switched to CO (3%CO in Ar). In the CO-DRIFTS experiments under vacuum, the reaction chamber was kept at 25 °C during the measurement. The reaction chamber was degassed under vacuum for 2 h. Then CO was dosed for 10 min (30 mL/min). The chamber was evacuated to remove the physical absorbed CO for 20 min and kept for vacuum for all the measurements.

2.4. Catalytic activity measurements

Typically, CO_2 hydrogenation reaction was operated in a 100 mL stainless-steel autoclave with temperature-control device. In a typical measurement, the catalyst was reduced under H_2/Ar (H_2/Ar=1:9) mixture with a flow rate of 30 mL/min for 2 h at 200 °C prior to reaction. The reaction chamber was flushed with feeding gas for three times. Then, 100 mg catalyst and 10 mL decalin was added to the chamber at room temperature (25 °C). Feeding gas of CO_2/H_2 mixture (H_2/CO_2 =3:1) was charged to the chamber to achieve specified pressure. The chamber was heated to the fix reaction temperature for specific time under magnetic stirring (600 rpm). Then the reaction chamber was cooled down in ice bath to room temperature. The product analysis procedure was similar to the reports previously [21,22]. The gas and liquid products were collected and analyzed by Shimadzu GC-2014 with a flame ionization detector. No liquid product was detected during all the tests. Therefore, the selectivity of product was calculated according to the composition of the gas products. Identity and quantitation of products were determined by external standard method calibrated by the standard gas mixture. The amount of input CO_2 was calculated by the online-calculators of the real gas state equations (http://www.energy.psu.edu/tools/CO2-EOS/index.php) based on the volume of the autoclave and the partital pressure of CO_2 in the charging mixture [23]. In the calculation of apparent activation barrier of CO_2 methanation, the reaction rate at different temperatures were calculated by fitting the conversion of CO_2 at even time intervals. During the cycling experiments, the solid catalyst was recycled by centrifugation and washed with deionized water for three times following by dried at 100 °C for 3 h in vacuum. Further details about the catalytic activity measurement is provided in the supporting material. The turnover number (TON) of the catalysts was defined as moles of CO_2 converted per mole surface Ru atom. The moles of surface Ru atom were calculated based on the content of Ru measured by ICP and the Ru dispersion.

2.5. Computational details

Spin polarized density function theory calculations were employed in the Vienna initio simulation package (VASP) with the Perdew-Burke-Ernzerh (PBE) exchange-correlation function [24]. Project augmented

wave (PAW) method was used to describe the interaction between the ions and valence electrons. The plane wave basis set has a cut-off energy of 400 eV. The t-ZrO_2 (101) surface was constructed by 2 × 2 supercell with the dimensions of 12.82 × 10.93 × 22.84 Å. The supercell includes three Zr layers with O atom layers on both sides. The slab model with ten atoms Ru cluster on the 2 × 2 supercell was reported to give reasonable results in previous calculations [25]. The bottom Zr layer was fix in its bulk structure while the top two layers with the Ru cluster and adsorbate molecule were allowed to fully relax. The optimal adsorption of alkali metals was screened by comparing the adsorption energies of alkali metals on various sites of Ru/ZrO_2. The model of Ru/M-ZrO_2 (M=Li, Na, K, and 2Na) was constructed by anchoring the corresponding alkali metals to the optimal adsorption site of Ru/ZrO_2. The electronic and geometric convergence criteria were 10^{-5} eV and 0.05 eV/Å, respectively. The vacuum thickness was set to 15 Å to ensure negligible interaction between periodic images [26]. To identify the interaction between adsorbed Na and Ru/ZrO_2 or the supported Ru cluster and ZrO_2, charge density difference isosurface was calculated by subtracting the charge density of the individual components from the total Ru/Na-ZrO_2 system, such as:

$$\Delta\rho_1 = \rho_{total} - \rho_{Na} - \rho_{Ru/ZrO2}$$

$$\Delta\rho_2 = \rho_{total} - \rho_{Ru} - \rho_{ZrO2}$$

3. Results and discussion

3.1. Catalyst characterization

To obtain the structure information of the alkali metal promoted Ru/ZrO_2 (Ru/M-ZrO_2, M = Li, Na, and K), the characterization results are analyzed firstly. In Fig. 1a, the calculated lattice parameter of Ru/ZrO_2 (a=b=3.606 Å, c=5.149 Å and $\alpha = \beta = \gamma = 90°$) allows the identification of tetragonal phase ZrO_2 (a=b=3.598 Å, c=5.152 Å and $\alpha = \beta = \gamma = 90°$ for JCPDS 88–1007), corresponding to P42/nmc space group [27]. Moreover, no Ru phase was observed in all samples, indicating the high dispersion and small particle size of Ru species on ZrO_2. The diffraction peaks position is nearly unaffected with the addition of different alkali metals. Therefore, the crystal phase of ZrO_2 is retained after the modification of alkali metal promoters on its surface. Owing to the feed ratio of Na is 1.00 wt%, the actual Na content over ZrO_2 surface could be lower. The signal of Na 1 s, Li 1 s, and K 2p orbital in the XPS spectra is weak (Fig. S1). The actual content of alkali metals in Ru/M-ZrO_2 (M=Li, Na and K) was further analyzed by ICP-OES (Table 1 and Table S1). The contents of Li, Na and K in the alkali metal promoted Ru/ZrO_2 are 0.23 wt%, 0.92 wt%, and 1.40 wt%, respectively, which are lower than the nominal values. It may be due to the loss in the preparation process. The loading amount of Ru is closed to the nominal ratio of 1.00 wt%. In addition, the surface area of Ru/ZrO_2 decreases slightly after the modification of alkali metals (Table 1).

The XPS spectras of Ru/ZrO_2 and alkali metal promoted Ru/ZrO_2

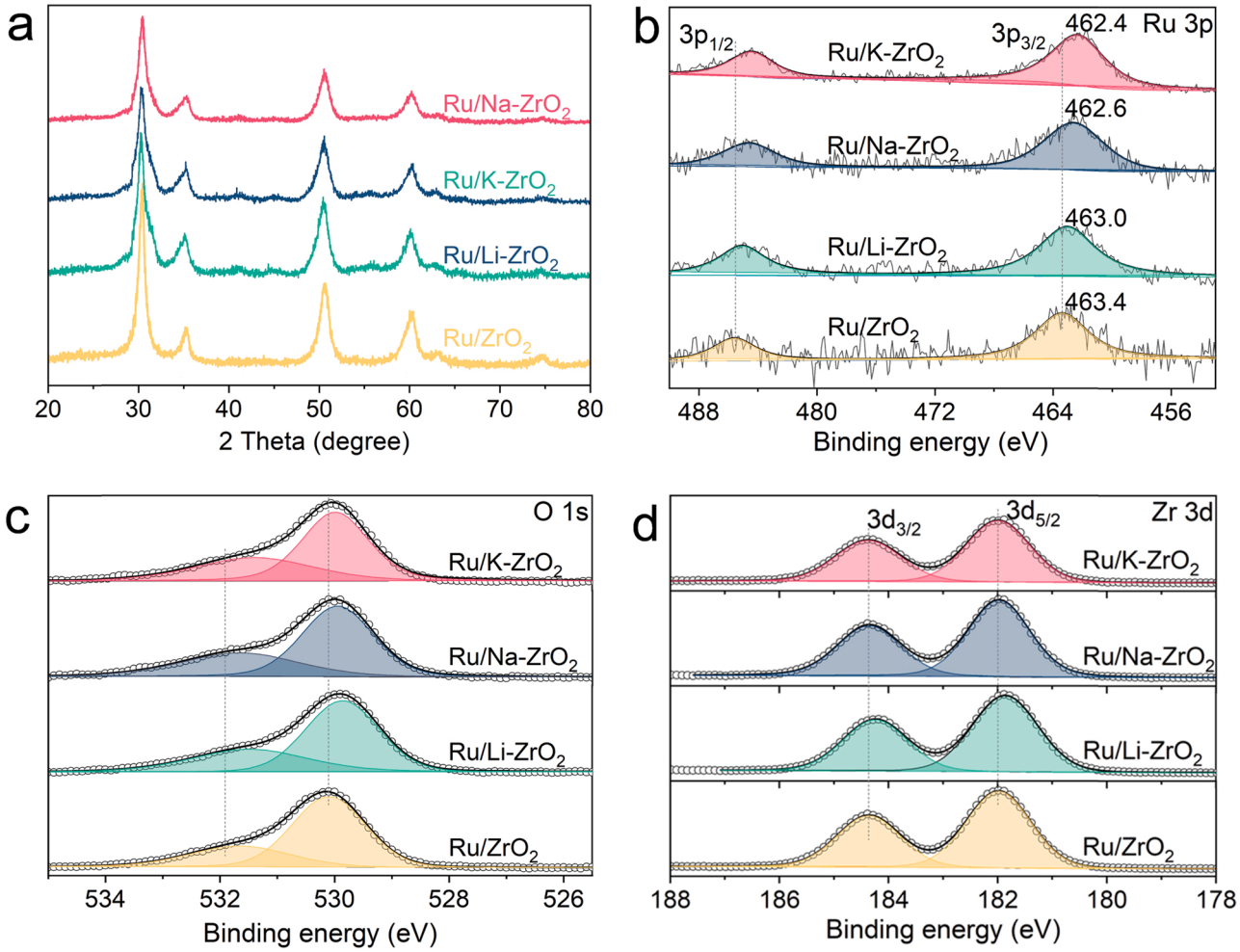

Fig. 1. (a) XRD patterns of Ru/ZrO_2 and alkali metal promoted Ru/M-ZrO_2 (M=Li, Na and K). XPS spectra of (b) Ru 3p, (c) O 1 s, and (d) Zr 3d in Ru/ZrO_2 and alkali metal promoted Ru/M-ZrO_2 (M=Li, Na and K).

Table 1
Physiochemical parameters of Ru/ZrO_2 and $Ru/M\text{-}ZrO_2$ (M=Li, Na and K).

Catalyst	Content of Ru (wt%)	Content of alkali metals (wt%)	Particle size of Ru (nm)	BET surface area (m^2/g)
Ru/ZrO_2	0.91	—	1.10	95.63
Ru/Li-ZrO_2	0.89	0.23	1.16	90.50
Ru/Na-ZrO_2	0.95	0.92	1.40	83.49
Ru/K-ZrO_2	0.97	1.40	1.34	86.01

were analyzed and shown in Fig. 1b-d. The XPS spectra of Zr 3d in Ru/ZrO_2 shows two characteristic peaks at 182.0 and 184.5 eV (Fig. 1d), which assigned to Zr $3d_{5/2}$ and Zr $3d_{3/2}$ of Zr^{4+} [28,29]. The peaks centered at 531.8 and 530.1 eV are ascribed to lattice oxygen of ZrO_2 (Fig. 1c) [30]. The binding energies of Zr 3d in alkali metal promoted Ru/ZrO_2 are nearly unchanged comparing with the alkali metal free Ru/ZrO_2. Additionally, the binding energies of O 1 s in alkali promoted Ru/ZrO_2 all shift towards lower energy levels slightly. In Ru/ZrO_2, the peaks at 463.4 and 485.6 eV are assigned to Ru $3p_{3/2}$ and Ru $3p_{1/2}$ of Ru^0 species (Fig. 1b) [31]. With the addition of alkali metals, the binding energies of Ru 3p orbital all shift to lower binding energies with the shift value increasing gradually by the sequence of Li, Na, and K. Consequently, the alkali metal promoters on ZrO_2 support may transfer electrons to Ru. The electron enrichment of Ru could affect the adsorption and reaction ability of intermediates. Hence, the performance of CO_2 hydrogenation could be regulated. It is concluded that the electron density of Ru centers and O in ZrO_2 is enriched by the donation effect of alkali metals, which agrees with the previous result [32].

Typical morphology and crystalline nature of Ru/ZrO_2 and alkali metal promoted Ru/ZrO_2 are explored by TEM examinations. In Fig. 2a and Fig. S2, the lattice spacing of ca. 0.30 nm in Ru/ZrO_2 and alkali metal promoted Ru/ZrO_2 matches well with the (101) plane of tetragonal ZrO_2 [33]. This is consistent with the observation of XRD characterization in Fig. 1a. An inter-planar lattice spacing of 0.22 nm is assigned to the hcp-Ru structure [34]. The morphology of these catalysts shows similar stack structure with Ru particles scattered on the surface of ZrO_2. The particle size of Ru in Ru/ZrO_2 and three alkali metal promoted Ru/ZrO_2 has comparable average diameters of ca. 1.10–1.40 nm (Fig. 2c-f and Table 1). And $Ru/Na\text{-}ZrO_2$ after cycle experiments shows no obvious change in the crystal phase of ZrO_2 and particle size of Ru (Fig. S4c). The EDX element mapping confirm the uniformly dispersion of Ru and Na species in $Ru/Na\text{-}ZrO_2$ (Fig. 2b). In brief, the crystallite size of Ru is not affected obviously by the addition of alkali metals.

3.2. *Catalytic performance of Ru/ZrO_2 and alkali metal promoted Ru/ZrO_2*

Hydrogenation of CO_2 was performed using Ru/ZrO_2 and $Ru/M\text{-}ZrO_2$ (M=Li, Na and K) under sets of conditions. Typically, the reaction was performed in a 100 mL stainless-steel autoclave under the pressure of 1.0 MPa (H_2:CO_2 =3:1) at 200 °C for 1.5 h. To explore the effects of alkali metal promoters, the conversion and selectivity in CO_2 methanation process over Ru/ZrO_2 and various alkali metal promoted Ru/ZrO_2 were analyzed. As indicated in Fig. 3a, the conversion over Ru/ZrO_2 was only 1.2% under the given reaction condition. Additionally, no conversion of CO_2 was observed in the case of merely ZrO_2. Notably, the conversion over alkali metal promoted Ru/ZrO_2 are all highly improved comparing with the unpromoted Ru/ZrO_2. Particularly, the conversion over $Ru/Na\text{-}ZrO_2$ (20.9%) is more than an order of magnitude higher than Ru/ZrO_2 (1.2%) and is also higher than the Li or K promoted ones (10.7% and 14.8%). In addition, the activity order of different alkali metal promoted Ru/ZrO_2 under H_2:CO_2 = 4:1 agrees with the results in

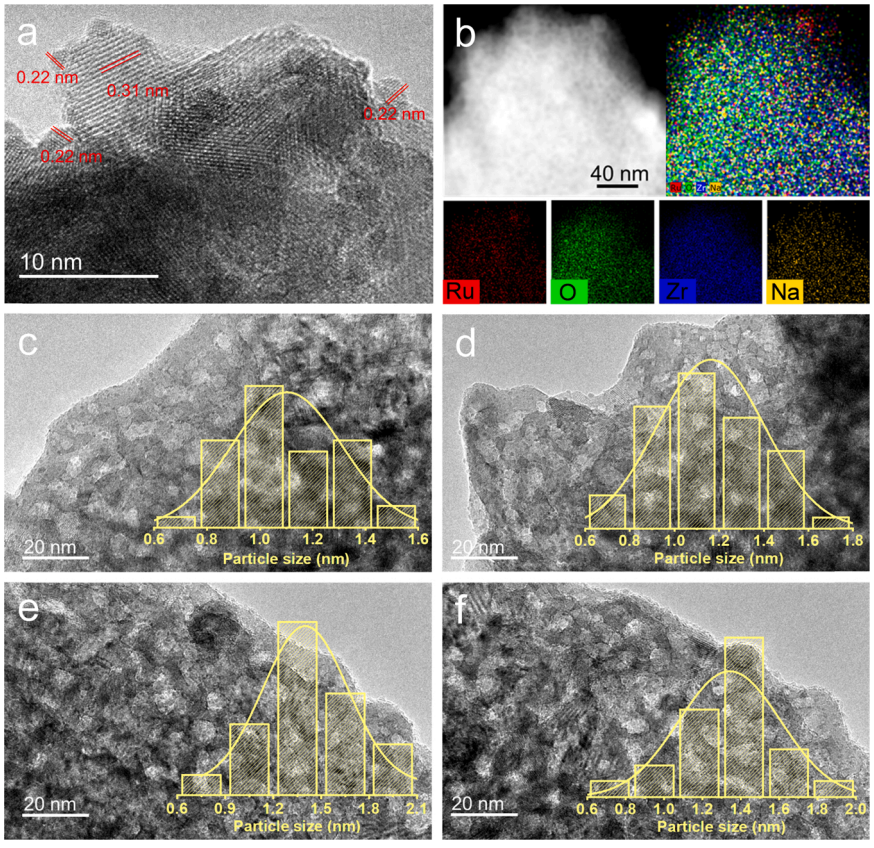

Fig. 2. (a) HRTEM images of $Ru/Na\text{-}ZrO_2$. (b) EDX mapping images of $Ru/Na\text{-}ZrO_2$. TEM images of (c) Ru/ZrO_2, (d) $Ru/Li\text{-}ZrO_2$, (e) $Ru/Na\text{-}ZrO_2$, and (f) $Ru/K\text{-}ZrO_2$. The inset is the corresponding Ru particle size distribution.

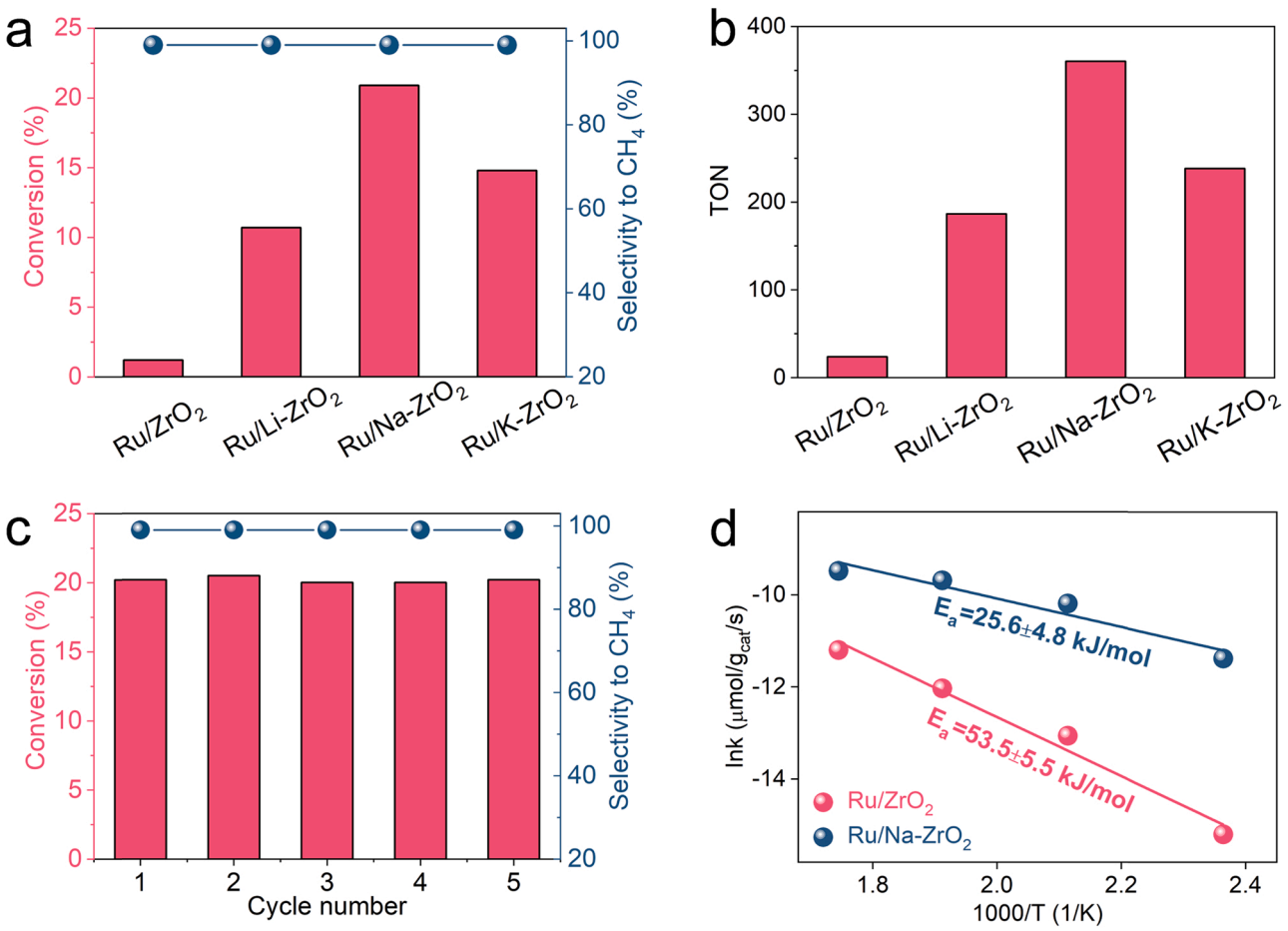

Fig. 3. CO_2 conversion (a) and TON (b) of Ru/ZrO_2 and alkali metal promoted samples under 200 °C. (c) Recycling experiments results of $Ru/Na\text{-}ZrO_2$. (d) Arrhenius plot of CO_2 conversion over Ru/ZrO_2 and $Ru/Na\text{-}ZrO_2$.

H_2:CO_2 = 3:1 (Fig. S17). In the cycling experiment, $Ru/Na\text{-}ZrO_2$ did not exhibit apparent activity loss after five runs (Fig. 3c). The conversion of $Ru/Na\text{-}ZrO_2$ (20.9% under 1 MPa at 200 °C) is higher than the reported conversion of Ru/ZrO_2 (11.3% under 4 MPa at 200 °C with the same H_2:CO_2 molar ratio) at much higher pressure under stainless-steel autoclave system [35]. The turnover number (TON) of the focus catalysts were analyzed based on the dispersion of Ru (calculation details seeing Table S12). As shown in Fig. 3b, the TON of Ru/ZrO_2 and $Ru/M\text{-}ZrO_2$ (M=Li, Na, and K) under 200 °C is 23.8, 186.7, 360.4, and 238.3, respectively. The TON of $Ru/Na\text{-}ZrO_2$ is higher than the reported values of Rh/CeO_2 (TON=221) in stainless-steel autoclave system under similar reaction conditions (CO_2:H_2 =1:3, 4 MPa, 200 °C) [36]. Under lower (150 °C) and higher temperatures (250 °C), the alkali metals promoted Ru/ZrO_2 samples show similar activity sequence which are all higher than the unpromoted Ru/ZrO_2 (Fig. S12). Further, the content of Na in $Ru/Na\text{-}ZrO_2$ was optimized. Fig. S4a shows that the highest conversion was achieved in $Ru/1.0Na\text{-}ZrO_2$. The conversion decreased when the Na content is higher or lower than 1.0 wt%. The selectivity to methane is 99% in all catalysts and less affected by the modification of alkali metals.

Further, the conversion of CO_2 at different temperatures on Ru/ZrO_2 and $Ru/Na\text{-}ZrO_2$ was collected. In Fig. S4b, the conversion of CO_2 over $Ru/Na\text{-}ZrO_2$ is higher than Ru/ZrO_2 under the tested temperatures (150–300 °C). The conversion of CO_2 over Na-promoted Ru/ZrO_2 increases sharply with the temperature increase. In order to understand the origin of the sharp increase of conversion by Na modification, the kinetic curve was obtained (Fig. 3d). The apparent activation barrier of CO_2 methanation over Na-promoted and Na-free Ru/ZrO_2 was calculated based on the reaction rate under different reaction temperatures by the Arrhenius equation. Obviously, the apparent activation energy of $Ru/Na\text{-}ZrO_2$ (25.6 ± 4.8 kJ/mol) is much smaller than that of Ru/ZrO_2 (53.5 ± 5.5 kJ/mol). The drop in apparent activation energy indicates that the activity improvement is caused by the improved efficiency of active sites upon Na promotion. Hereafter, the promotional effects of Na were investigated in details.

3.3. *Probing the hydrogenation process*

To further understand the surge improvement of activity upon Na addition, the CO_2 reduction process over Ru/ZrO_2 and $Ru/Na\text{-}ZrO_2$ was explored by in-situ DRIFTS. The samples were pretreated by Ar atmosphere at 200 °C for 2 h. Then, CO_2/H_2 mixture was introduced into the sample cell to probe the adsorption behavior on the ZrO_2 support. In the absence of H_2 dissociation sites, CO_2 is adsorbed with the appearance of bands at 1620, 1560, and 1440 cm^{-1} (Fig. 4a). The bands at 1620 and 1440 cm^{-1} are attributed to bicarbonate species (HCO_3^-) while the band centered at 1560 cm^{-1} is identified as carboxylate species ($COOH^-$) [37, 38]. Dissociation of CO_2 to CO does not occur under this condition owing to the absence signals of CO* at 1900–2100 cm^{-1} (Fig. S5). With the addition of Ru, the bands of CO species appear, which indicate the dissociation of CO_2 happens (Fig. 4b). CO_2-TPD was also conducted to explore the adsorption behavior of CO_2 on Ru/ZrO_2 and $Ru/Na\text{-}ZrO_2$ [39]. In Fig. S6, the addition of Na mainly increases the intensity of CO_2 on the medium basic sites (ca. 320 °C, corresponding to bidentate carbonates species). The intensity at lower temperature (ca. 150 °C, corresponding to bicarbonate species) was not superior. In the light of the in-situ DRIFTS results (Fig. 4b and e), the band intensity of carbonates species (1350–1370 cm^{-1}) shows little change during the CO_2

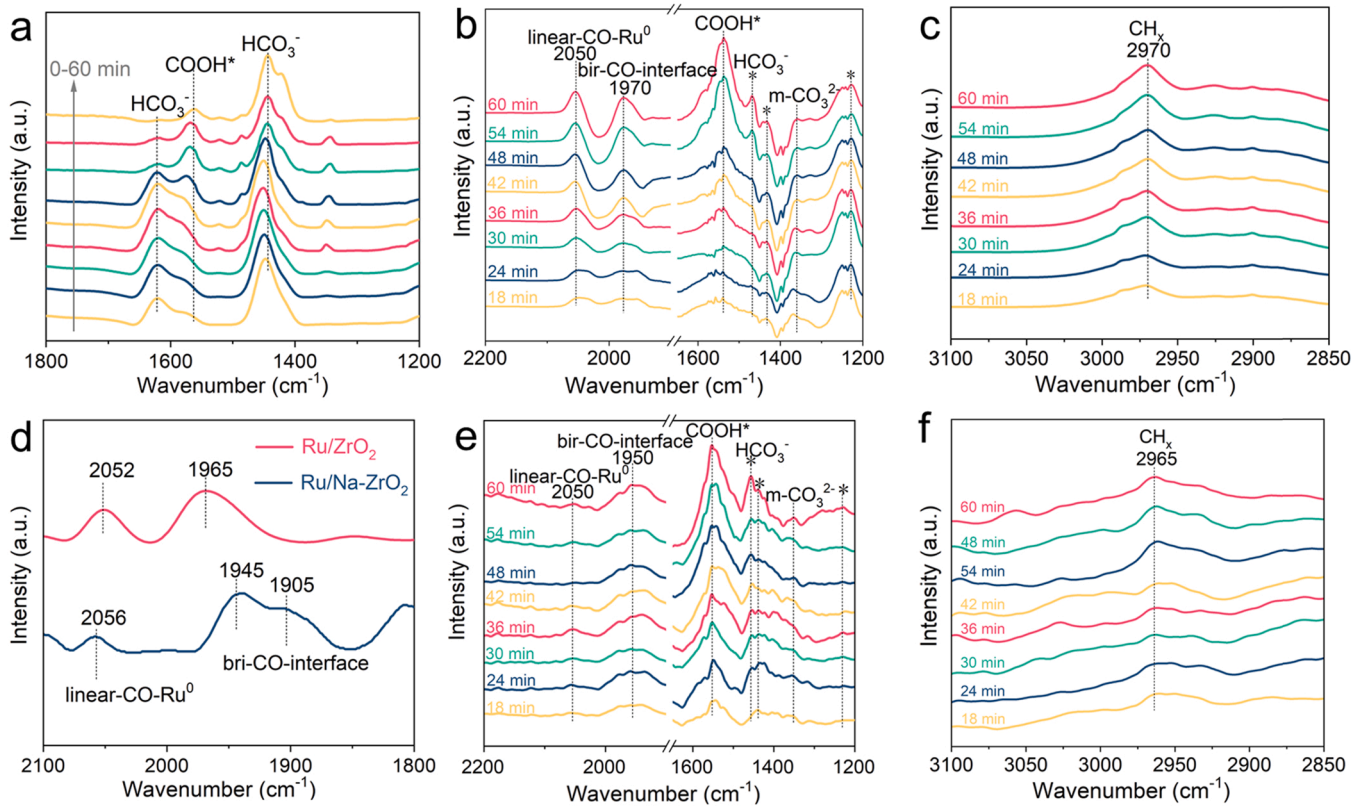

Fig. 4. (a) Time-dependent in-situ DRIFT spectra of ZrO_2 under flowing of CO_2/H_2 mixture. Time-dependent in-situ DRIFT spectra of Ru/ZrO_2 (b and c) and $Ru/Na-ZrO_2$ (e and f) with flowing of CO_2/H_2 mixture. (d) DRIFT spectra of Ru/ZrO_2 and $Ru/Na-ZrO_2$ with flowing of 3%CO in Ar.

methanation process, which could be the spectator of the hydrogenation process. The improved adsorption of CO_2 at medium basic sites (as carbonates species) may not be the decisive factor for the high conversion of CO_2. Therefore, the promotion effect of Na is not likely due to the enhanced CO_2 chemisorption as proposed by Liu et al. [40].

In the in-situ DRIFTS results, we focus on the bands at 1200–2200 cm^{-1} because the key reaction intermediates are detected in this range [41]. For Ru/ZrO_2 (Fig. 4b and c), the bands lower than 1600 cm^{-1} are identified as carboxylate (1540 cm^{-1}), bicarbonate species (1463, 1430, and 1230 cm^{-1}), and monodentate carbonate species (1370 cm^{-1}) with the injection of CO_2 and H_2 mixture [42,43]. The high increasing intensity of band at ca. 1540 cm^{-1} indicates the dominant adsorption mode of CO_2 is carboxylate on Ru/ZrO_2 surface, which may be the precursor of CO intermediate. The bands at 1970 and 2050 cm^{-1} are attributed to bridge adsorbed CO at the metal-support interfacial sites (bri-CO-interfacial) and linearly bonded CO on Ru^0 sites (linear-CO-Ru^0), respectively [14,44,45]. As indicate in Fig. 4b, the signal of linearly bonded CO on Ru^0 sites is higher than bridge CO at interfacial sites. In Fig. 4c, the band at 2970 cm^{-1} is assigned to C-H vibrations frequency of alkane species (CH_x *) [46], indicating the generation of methane. From the above evidences, CO_2 methanation proceed through the dissociation of CO_2 * to CO* following by hydrogenation of CO* to CH_x * and then CH_4.

Over $Ru/Na-ZrO_2$ surface (Fig. 4e and f), carboxylate (1550 cm^{-1}), bicarbonate species (1458, 1432, and 1230 cm^{-1}), and monodentate carbonate species (1350 cm^{-1}) were also detected similar to that in Ru/ZrO_2 with the flowing of gas mixture. In striking contrast, bands belong to adsorbed CO are mainly centered at 1950 cm^{-1} with rather weak peak intensity at 2050 cm^{-1}, indicating the major adsorption mode of CO is changed into bridge adsorption at the metal-support interfacial sites over Na promoted Ru/ZrO_2 surface. Therefore, the addition of Na could change the adsorption of CO intermediate. Afterwards, DRIFTS with flowing of CO (3%CO in Ar) was performed to explore the adsorption behavior of CO on Ru/ZrO_2 and $Ru/Na-ZrO_2$ surface (Fig. 4d). On Ru/ZrO_2, the band intensity of bridge adsorbed CO on the interfacial sites at 1965 cm^{-1} is comparable to the band intensity of linearly adsorbed CO on Ru^0 sites at 2052 cm^{-1}. However, over $Ru/Na-ZrO_2$ surface, the band intensity of bridge adsorbed CO at lower frequency (1905 and 1945 cm^{-1}) is much higher than the linearly adsorbed CO at Ru^0 (at 2056 cm^{-1}). This phenomenon verifies the results of the in-situ DRIFTS under the reaction atmosphere over the two catalysts, indicating that the adsorption behavior of CO on Ru/ZrO_2 is perturbed by the addition of Na indeed. Besides, owing to the discrepancy in the reaction atmosphere over the two measurements (CO_2/H_2 mixture or CO), the bands positions and relative bands intensity of CO are not completely consistent. However, it does not obstruct the qualitative comparison of the CO adsorption behavior. In addition, the DRIFT spectra of CO adsorption under vacuum also indicates that the addition of Na increases the adsorption of CO on the interfacial Ru site (Fig. S13). It could be observed from the CO-TPD spectra that the modification of Na enhances the adsorption strength of strong absorbed CO on Ru sites (Fig. S14). Further, the discrepancy in CO adsorption under the reaction atmosphere was also observed on Li/K promoted Ru/ZrO_2 under reaction atmosphere (Fig. S7). The bands intensity at ca. 1950 cm^{-1} are higher than that centered at 2050 cm^{-1} in Li and K promoted Ru/ZrO_2. But the difference is not as obvious as the Na promoted catalyst. Although changes of CO adsorption behavior by the modification of alkali metals are observed in the DRIFTS, the infrared spectrum is not an optimal choice for the quantitative analysis of CO adsorption. Density functional theory (DFT) calculations could provide atomic level information about the modified surface, which is conducive to tracking and understanding the resulting changes in the adsorption and reaction behavior of intermediates in the catalytic process. Consequently, aiming to further identify the effect of alkali metal addition on the behavior of Ru/ZrO_2 in CO_2 hydrogenation, DFT calculations were performed.

3.4. DFT calculations

To identify the optimum adsorption configurations of Na on Ru/ZrO_2 surface, the adsorption of Na on various sites of Ru/ZrO_2 are examined. The adsorption configurations and corresponding adsorption energies are shown in Fig. S8 and Table S2. The most preferable adsorption site of Na is the O-hollow site of ZrO_2 close to the Ru cluster (Fig. 5a and b). Bader charge analysis shows that the atomic net charge of Na in $Ru/Na\text{-}ZrO_2$ is 0.85 |e|, indicating that Na is an electron donor in $Ru/Na\text{-}ZrO_2$ [47].

Further charge analysis shows that both the O atoms in the ZrO_2 support and the Ru center are electron acceptors, with the latter being the dominant one. The total charge of the top layer O atoms in $Ru/Na\text{-}ZrO_2$ is 0.2 |e| higher than that in Ru/ZrO_2, indicating the electron enrichment of the top layer O atoms with Na promotion (Fig. S9 and Table S3). On the other hand, the charge of the Ru cluster is − 0.32 |e| in Ru/ZrO_2, and − 0.75 |e| in $Ru/Na\text{-}ZrO_2$ (Table S3). Therefore, the Ru cluster is also more electron-rich on Na promoted Ru/ZrO_2 surface than the unpromoted one. This prediction is in accordance with the negative shift of the binding energies of Ru 3p and O 1 s in the XPS spectra (Fig. 1b and c).

Moreover, besides Na promotion, the charge of the Ru clusters in Li and K promoted Ru/ZrO_2 are also increased, being − 0.66 |e| and − 0.79 |e|, respectively. The predicted trend of electron enrichment of Ru center upon different alkali metal promotion (Li-promoted < Na-promoted < K-promoted) coincides with the experimental trend, which is signaled by the extent of binding energy shift of Ru 3p orbital in the XPS spectra of Fig. 1b. However, this trend disagrees with the observed trend of catalytic activity (Li-promoted < K-promoted < Na-promoted). The best activity is achieved in Na promoted Ru/ZrO_2. Therefore, the electron enrichment of Ru cluster is not the decisive factor for the activity difference upon different alkali metals addition.

To further identify the electronic effects of Na, the charge density difference plots are provided in Fig. 5c and d. It is clear that charge transfers from Na to Ru/ZrO_2, leading to a more electron-rich interface which could potentially serve as active sites for CO_2 methanation process. Besides, no obvious charge redistribution between the Ru cluster and the ZrO_2 support are observed with the addition of Na (Fig. S10). Therefore, the enriched charge density at the interfacial region of Ru/ZrO_2 with Na addition is mainly caused by the direct charge transfer from Na.

Further, the adsorption behavior of CO_2 and CO on Ru/ZrO_2 and $Ru/Na\text{-}ZrO_2$ was investigated. CO_2 can be adsorbed both on Ru cluster and at the Ru/ZrO_2 interface (Fig. 6a). On the Ru cluster, CO_2 has a tridentate adsorption state (top-Ru), whereas at the Ru/ZrO_2 interface, the adsorption of CO_2 may coordinate with either two interfacial Ru sites (int-Ru-Ru) or with one Ru and one Zr (int-Ru-Zr). With the addition of Na, the adsorption strength of CO_2 at top-Ru and int-Ru-Ru sites increased slightly by 0.18 eV and 0.30 eV, respectively. Notably, however, the adsorption at the int-Ru-Zr site increased by 1.38 eV with Na promotion. Therefore, the Na promotion mainly increased the adsorption strength of CO_2 at the Ru/ZrO_2 interfacial sites.

Similarly, a remarkable enhancement of the adsorption at the interfacial sites for the CO intermediate was also discovered. (Fig. 6b). Herein, only the adsorptions of CO on top-Ru site and near interfacial sites (int-Ru-Ru, and int-Ru-Zr) are considered, as signaled by the evidences of DRIFTS spectra in Fig. 4. Consistent with the DRIFTS signals, CO adsorption on top-Ru site takes a linear configuration, whereas its adsorptions at both int-Ru-Ru site and int-Ru-Zr sites have a bridge configuration. With the addition of Na, the increase of adsorption energy on these three sites are 0.40 eV, 0.43 eV, and 0.53 eV, respectively. Apparently, the adsorption strength of CO near the interfacial sties increases more significantly with the modification of Na, particularly with the Ru-Zr bridge adsorption configuration. The calculated CO adsorption behavior provides further evidence, in addition to the observed in-situ DRIFTS results, that Na promoted is conducive to the adsorption of bridge CO near the interfacial sites of Ru/ZrO_2.

It has been reported that the cleavage of the second C-O bond of CO_2 is the rate-limiting step in CO_2 methanation over Ru based catalyst [48]. To confirm this, the energy barriers for cleaving the C-O bond of CO_2 and CO on different sites of Ru/ZrO_2 are calculated. Results show that the energy barriers for cleaving the C-O bond of CO_2 (0.41–1.12 eV) are

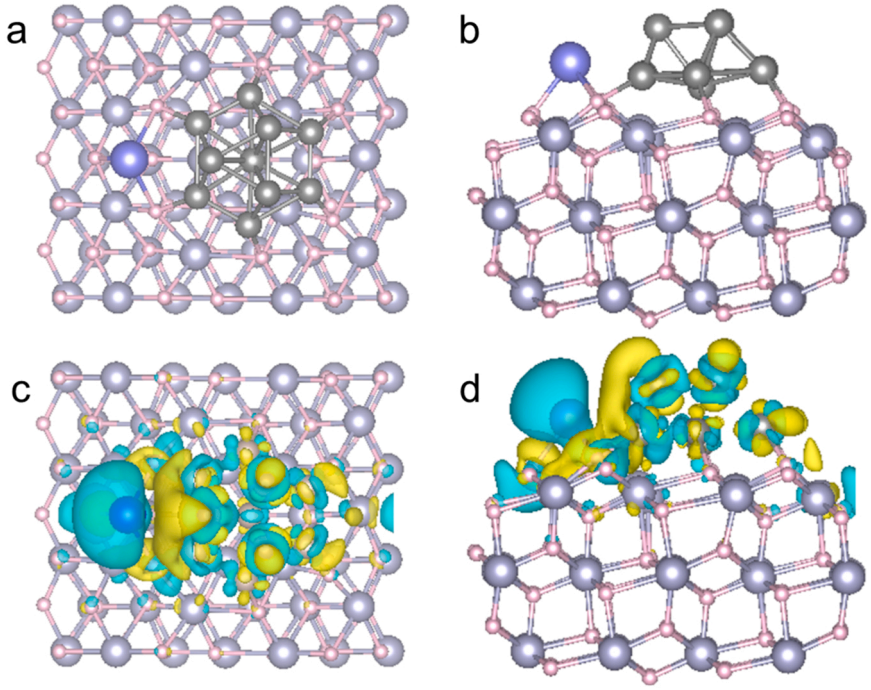

Fig. 5. Stable adsorption site of Na on Ru/ZrO_2 in top (a) and side view (b). Charge density difference plot ($\Delta\rho_1$) of Na in $Ru/Na\text{-}ZrO_2$ with the isovalue value of 0.008 e/Å^3 in top (c) and side view (d). The yellow region represents charge accumulation while blue region indicates charge depletion. The ball in gray, pink, purple, light purple represents Ru, O, Na, and Zr atoms.

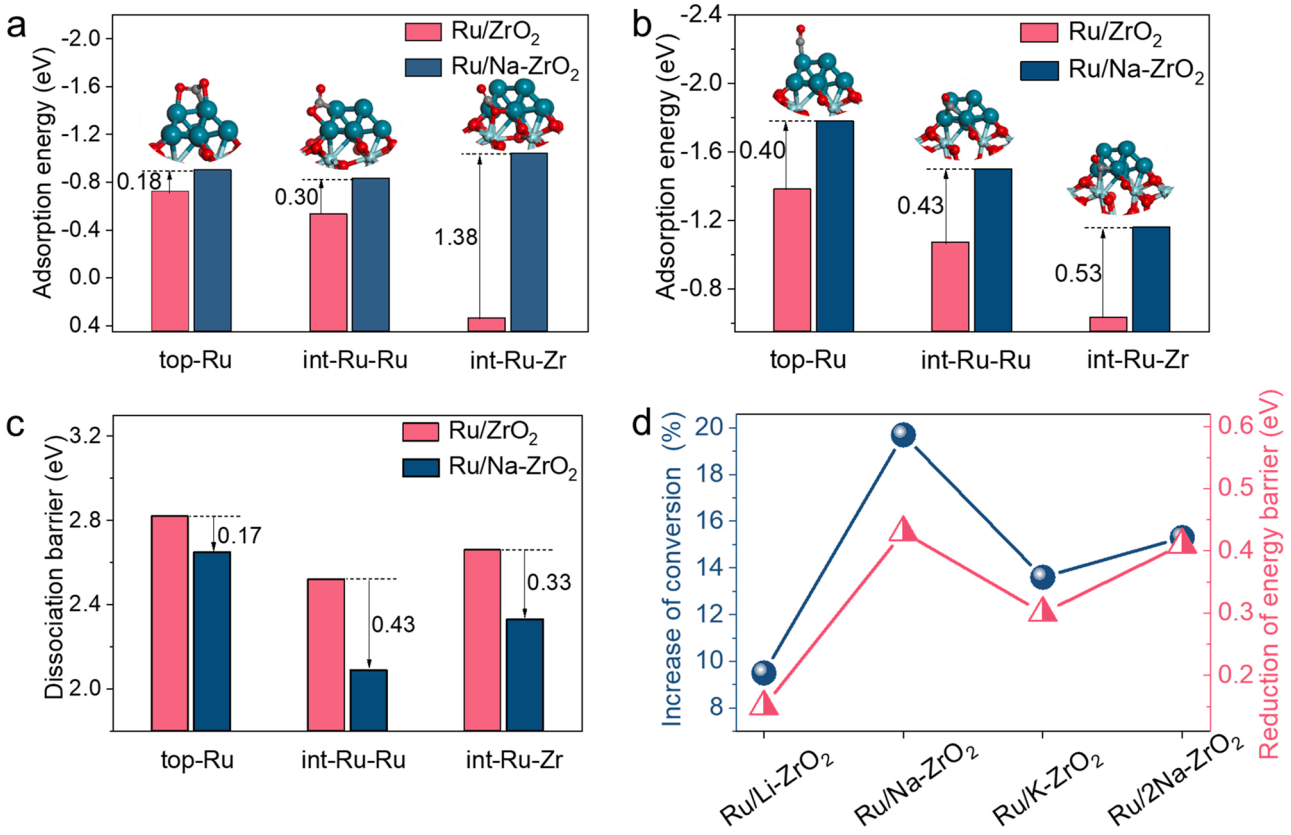

Fig. 6. Adsorption configurations and adsorption energies of CO_2 (a) and CO (b) on Ru/ZrO_2 and $Ru/Na\text{-}ZrO_2$ (The adsorption energies are provided in Table S5 and S6). (c) Dissociation barriers of CO on Ru/ZrO_2 and $Ru/Na\text{-}ZrO_2$ (seeing Table S7). (d) Correlation of the reduction of CO dissociation barrier on the site with lower CO dissociation barrier and the increase of CO_2 conversion over Ru/ZrO_2 and alkali metal promoted Ru/ZrO_2.

much lower than that in CO (2.52–2.82 eV) (Table S4 and Table S7). Therefore, the high energy cost in cleaving the C-O bond of CO determines the activity of CO_2 methanation over Ru/ZrO_2, and deserves further analysis.

On unpromoted Ru/ZrO_2, CO on the top-Ru site has an extremely high dissociation barrier of 2.8 eV. Thus, although it is a favorable site for CO adsorption, the methanation reaction is unlikely to happen on this site. The two types of interfacial sites (int-Ru-Ru and int-Ru-Zr site) have similar barrier for CO dissociation, both are lower than the top-Ru site (Table S7). Projected density of states (PDOS) and Crystal Orbital Hamilton Populations (COHP) analysis shows that the C-O bond can be weakened most significantly on these interfacial sites, reflected by the increasing population of CO π-metal $d\pi$ hybrid band () in pDOS and the weakened C-O bond in the integrated crystal orbital Hamilton population (ICOHP) (Fig. 7a and c, and Fig. S11a). With Na modification, the dissociation barrier of C-O bond of linearly absorbed CO on top-Ru site of $Ru/Na\text{-}ZrO_2$ only decreases by 0.17 eV. At int-Ru-Zr site, the barriers decrease by 0.33 eV. It is worth noting that the int-Ru-Ru site features the most significant decline of the CO dissociation barrier by 0.43 eV (Fig. 6c). To further trace the origin of the drastic decline in CO dissociation barriers on int-Ru-Ru and int-Ru-Zr site by Na modification, the electronic structure of the absorbed CO is analyzed. Comparing with the unpromoted surface, there is less charge deficiency in the absorbed CO on the interfacial sites of Na promoted surface (net charge from 0.26 |e| to 0.29 |e| on top-Ru site, from 0.39 |e| to 0.59 |e| on int-Ru-Ru site and from 0.53 |e| to 0.82 |e| on int-Ru-Zr site, seeing Table S9), indicating a stronger electron back-donation from the interfacial sites to the absorbed CO. Moreover, the population of $\bar{d}\pi$ band, which is responsible for the electron back-donation to CO, increases with Na addition (Fig. 7). These evidences confirm the enhancement of electron back-donation from the int-Ru-Ru and int-Ru-Zr site to the absorbed CO, promoting the activation of the absorbed CO [49]. Therefore, the Na promotion most likely works by reducing the dissociation barrier of the CO intermediate on the interfacial sites of Ru/ZrO_2 through the enhancement of the electron back-donation.

According to the previous reports of the supported Ru catalysts on metal oxide supports [50–52], the interfacial sites play vital roles in the adsorption and activation of CO intermediate in the methanation of CO_2, which contributes to the catalytic activity improvement. Herein, the decrease dissociation barrier of CO at the int-Ru-Ru and int-Ru-Zr site could be important contributors to the activity increase upon the modification of alkali metals (Fig. S18). Therefore, the reduction of CO dissociation barrier on the site with lower energy barrier should be a more reasonable indicator in assessing the activity of different alkali metal promoted Ru/ZrO_2. The reduction of CO dissociation barrier on the site with lower CO dissociation barrier were plotted against the experimental conversion increase of CO_2 (Fig. 6d and Table S8). Remarkably, the increase in the conversion of CO_2 on different alkali metal promoted Ru/ZrO_2 is found to be related to the decrease of CO dissociation barriers at the interfacial site. Therefore, the dissociation barrier of CO at the interfacial site could be used as an indicator in assessing the CO_2 methanation activity of alkali metals promoted Ru/ZrO_2. The difference in the reduction of CO dissociation barrier upon Li, Na, and K promotion could be explained by the difference in the enhancement of the electron back-donation effect from the interfacial sites to the absorbed CO (Table S10 and Fig. S16).

4. Conclusions

To reveal the promotional effects of alkali metals on the CO_2 hydrogenation behavior of Ru/ZrO_2, the performance of Ru/ZrO_2 and alkali metal promoted $Ru/M\text{-}ZrO_2$ (M=Li, Na, and K) are explored by

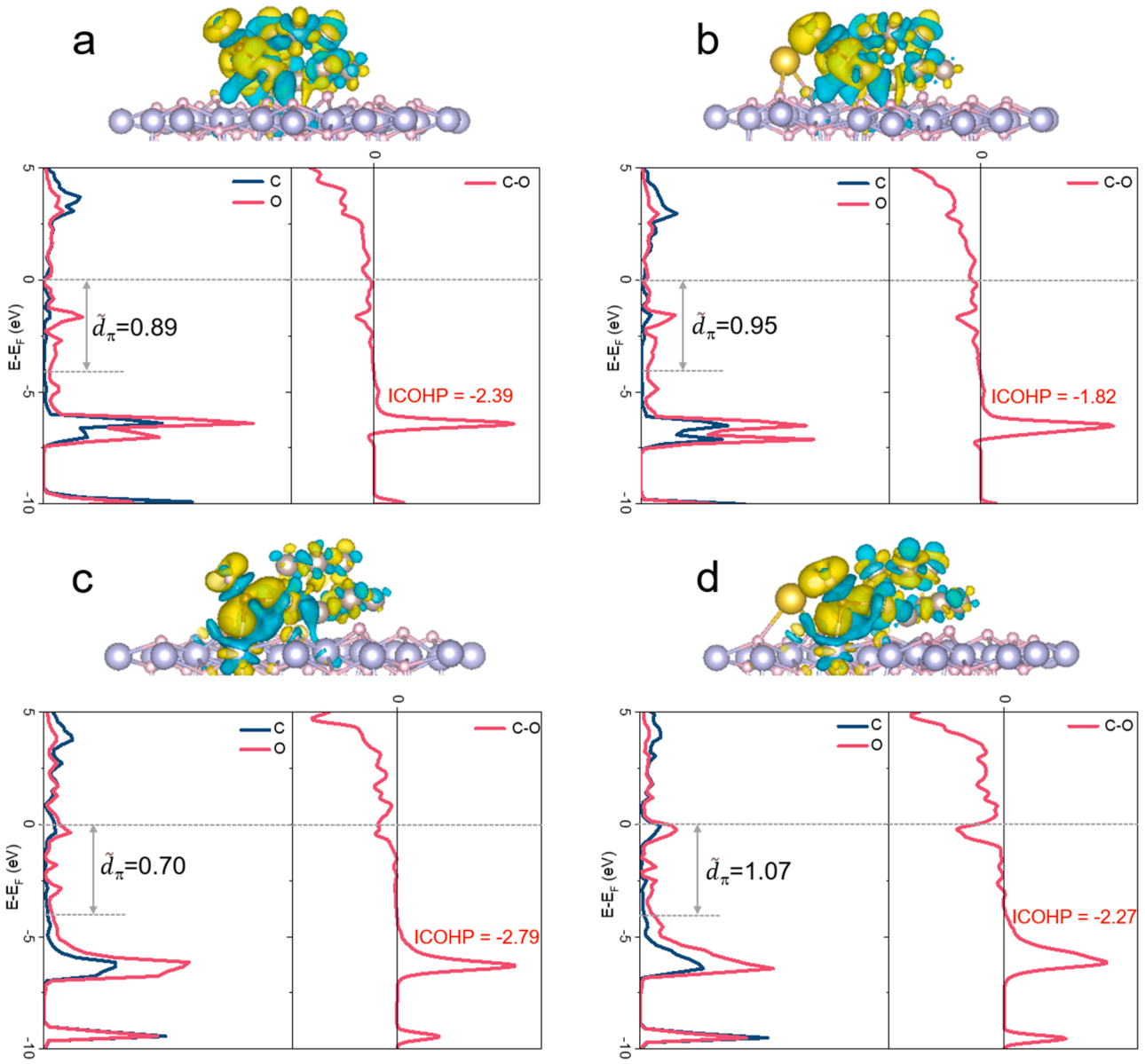

Fig. 7. Charge density difference isosurface of absorbed CO on int-Ru-Ru site and int-Ru-Zr site of Ru/ZrO_2 (a and c) and Ru/Na-ZrO_2 (b and d) with the according project density of states (pDOS) and projected crystal orbital Hamilton population (pCOHP) curves shown below.

experimental and theoretical measurements. The charge density of Ru in Ru/ZrO_2 increases by the order of unpromoted- < Li-promoted < Na-promoted < K-promoted, while the highest activity is achieved in Na-promoted ones. By probing the CO_2 hydrogenation process over Ru/ZrO_2 and alkali metal promoted Ru/M-ZrO_2, the promotional effects of alkali metals on the electronic structure and evolution of intermediates were revealed. We have proven that the alkali metals enrich the charge density of the metal-support interfacial region, and the adsorption strengths of CO_2 and CO are both enhanced. Although the population of linearly absorbed CO on top Ru site is higher than that of bridge CO near the interfacial site of the unpromoted Ru/ZrO_2, both of these adsorptions have high dissociation barriers. It is noted that the bridge absorbed CO near the int-Ru-Ru and int-Ru-Zr site is more favored with the addition of alkali metals with much lower dissociation barriers, which originate from the enhanced electron back-donation from the interfacial Ru sites to the absorbed CO. The increase in the conversion of CO_2 on different alkali metals promoted Ru/ZrO_2 is found to be more related to the enhanced back-donation to CO at the local interfacial sites, rather than the enriched charge density of Ru cluster as a whole. These findings may shed light on the reaction mechanism of CO_2 hydrogenation and guide the design of highly efficient catalysts by alkali metal promoters.

CRediT authorship contribution statement

Mengting Gao: Conceptualization, Methodology, Investigation, Writing – original draft, Visualization, Software. **Jin Zhang:** Investigation. **Pengqi Zhu:** Writing – review & editing. **Xingchen Liu:** Writing – review & editing, Software, Supervision. **Zhanfeng Zheng:** Writing – review & editing, Supervision.

Declaration of Competing Interest

The authors declare that they have no known competing financial interests or personal relationships that could have appeared to influence the work reported in this paper.

Acknowledgements

We appreciate the financial support from the National Natural Science Foundation of China (No. 22072176, 21603259) and the Hundred Talents Program of the Chinese Academy of Sciences and Shanxi Province. The theoretical calculations were performed at Shanxi Supercomputing Center of China, and the calculations were performed on TianHe-2.

Appendix A. Supporting information

Supplementary data associated with this article can be found in the online version at doi:10.1016/j.apcatb.2022.121476.

References

[1] Y. Wang, Q. Zhou, Y. Zhu, D. Xu, High efficiency reduction of CO_2 to CO and CH_4 via photothermal synergistic catalysis of lead-free perovskite $Cs_3Sb_2I_9$, Appl. Catal. B Environ. 294 (2021), 120236.
[2] J. Ashok, S. Pati, P. Hongmanorom, Z. Tianxi, C. Junmei, S. Kawi, A review of recent catalyst advances in CO_2 methanation processes, Catal. Today 356 (2020) 471–489.
[3] X. Hu, Z. Xie, Q. Tang, H. Wang, L. Zhang, J. Wang, Enhanced CH_4 yields by interfacial heating-induced hot water steam during photocatalytic CO_2 reduction, Appl. Catal. B Environ. 298 (2021), 120635.
[4] C. Vogt, M. Monai, G.J. Kramer, B.M. Weckhuysen, The renaissance of the Sabatier reaction and its applications on Earth and in space, Nat. Catal. 2 (2019) 188–197.
[5] W.D. Mross, Alkali doping in heterogeneous catalysis, Catal. Rev. 25 (2006) 591–637.
[6] F.J. Williams, A. Palermo, S. Tracey, M.S. Tikhov, R.M. Lambert, Electrochemical promotion by potassium of the selective hydrogenation of acetylene on platinum: Reaction studies and XP spectroscopy, J. Phys. Chem. B 106 (2002) 5668–5672.
[7] N. Boreriboon, X. Jiang, C. Song, P. Prasassarakich, Higher hydrocarbons synthesis from CO_2 hydrogenation over K- and La-promoted Fe–Cu/TiO_2 catalysts, Top. Catal. 61 (2018) 1551–1562.
[8] N. Mahata, K.V. Raghavan, V. Vishwanathan, Influence of alkali promotion on phenol hydrogenation activity of palladium alumina catalysts, Appl. Catal. A Gen. 182 (1999) 183–187.
[9] R. Qin, L. Zhou, P. Liu, Y. Gong, K. Liu, C. Xu, Y. Zhao, L. Gu, G. Fu, N. Zheng, Alkali ions secure hydrides for catalytic hydrogenation, Nat. Catal. 3 (2020) 703–709.
[10] B. Zugic, S. Zhang, D.C. Bell, F.F. Tao, M. Flytzani-Stephanopoulos, Probing the low-temperature water-gas shift activity of alkali-promoted platinum catalysts stabilized on carbon supports, J. Am. Chem. Soc. 136 (2014) 3238–3245.
[11] D. Heyl, U. Rodemerck, U. Bentrup, Mechanistic study of low-temperature CO_2 hydrogenation over modified Rh/Al_2O_3 catalysts, ACS Catal. 6 (2016) 6275–6284.
[12] W. An, F. Xu, D. Stacchiola, P. Liu, Potassium-induced effect on the structure and chemical activity of the Cu_xO/Cu(1 1 1) ($x \leq 2$) surface: a combined scanning tunneling microscopy and density functional theory study, ChemCatChem 7 (2015) 3865–3872.
[13] I. Kalaitzidou, M. Makri, D. Theleritis, A. Katsaounis, C.G. Vayenas, Comparative study of the electrochemical promotion of CO_2 hydrogenation on Ru using Na^+, K^+, H^+ and O^{2-} conducting solid electrolytes, Surf. Sci. 646 (2016) 194–203.
[14] P. Panagiotopoulou, Methanation of CO_2 over alkali-promoted Ru/TiO_2 catalysts: II. Effect of alkali additives on the reaction pathway, Appl. Catal. B Environ. 236 (2018) 162–170.
[15] F. David, M. Ollis, AlbertVannice, The catalytic synthesis of hydrocarbons from H_2/CO mixtures over the group VIII metals: comment on methanation kinetics, J. Catal. 38 (1975) 514–515.
[16] T. Witoon, J. Chalorngtham, P. Dumrongbunditkul, M. Chareonpanich, J. Limtrakul, CO_2 hydrogenation to methanol over Cu/ZrO_2 catalysts: effects of zirconia phases, Chem. Eng. J. 293 (2016) 327–336.
[17] D. Xu, M. Ding, X. Hong, G. Liu, Mechanistic aspects of the role of K promotion on Cu–Fe-based catalysts for higher alcohol synthesis from CO_2 hydrogenation, ACS Catal. 10 (2020) 14516–14526.
[18] C. Liu, W. Wang, Y. Xu, Z. Li, B. Wang, X. Ma, Effect of zirconia morphology on sulfur-resistant methanation performance of MoO_3/ZrO_2 catalyst, Appl. Surf. Sci. 441 (2018) 482–490.
[19] P. Zhu, M. Gao, J. Zhang, Z. Wu, R. Wang, Y. Wang, E.R. Waclawik, Z. Zheng, Synergistic interaction between Ru and MgAl-LDH support for efficient hydrogen transfer reduction of carbonyl compounds under visible light, Appl. Catal. B Environ. 283 (2021), 119640.
[20] L. Wang, L. Wang, J. Zhang, X. Liu, H. Wang, W. Zhang, Q. Yang, J. Ma, X. Dong, S. J. Yoo, J.G. Kim, X. Meng, F.S. Xiao, Selective hydrogenation of CO_2 to ethanol over cobalt catalysts, Angew. Chem. Int. Ed. 57 (2018) 6104–6108.
[21] Y. Chai, L. Li, J. Lu, D. Li, J. Shen, Y. Zhang, J. Liang, X. Wang, Germanium-substituted Zn_2TiO_4 solid solution photocatalyst for conversion of CO_2 into fuels, J. Catal. 371 (2019) 144–152.
[22] S. Bai, Q. Shao, P. Wang, Q. Dai, X. Wang, X. Huang, Highly active and selective hydrogenation of CO_2 to ethanol by ordered Pd-Cu nanoparticles, J. Am. Chem. Soc. 139 (2017) 6827–6830.
[23] B. An, Z. Li, Y. Song, J. Zhang, L. Zeng, C. Wang, W. Lin, Cooperative copper centres in a metal–organic framework for selective conversion of CO_2 to ethanol, Nat. Catal. 2 (2019) 709–717.
[24] G. Kresse, J. Furthmüller, Efficient iterative schemes for ab initio total-energy calculations using a plane-wave basis set, Phys. Rev. B 54 (1996) 11169–11186.
[25] H.-Y.T. Chen, S. Tosoni, G. Pacchioni, Adsorption of ruthenium atoms and clusters on anatase TiO_2 and tetragonal ZrO_2(101) surfaces: a comparative DFT study, J. Phys. Chem. C 119 (2014) 10856–10868.
[26] M. Gao, H. Tan, P. Zhu, J. Zhang, H. Wang, X. Liu, Z. Zheng, Why phenol is selectively hydrogenated to cyclohexanol on Ru (0001): an experimental and theoretical study, Appl. Surf. Sci. 558 (2021), 149880.
[27] S. Wang, J. Li, M. Zhang, P. Bai, H. Zhang, X. Tong, The selective reductive amination of aliphatic aldehydes and cycloaliphatic ketones with tetragonal zirconium dioxide as the heterogeneous catalyst, Mol. Catal. 494 (2020), 111108.
[28] T. Nishino, M. Saruyama, Z. Li, Y. Nagatsuma, M. Nakabayashi, N. Shibata, T. Yamada, R. Takahata, S. Yamazoe, T. Hisatomi, K. Domen, T. Teranishi, Self-activated Rh-Zr mixed oxide as a nonhazardous cocatalyst for photocatalytic hydrogen evolution, Chem. Sci. 11 (2020) 6862–6867.
[29] W. Zhu, A. Fujiwara, N. Nishiike, S. Nakashima, H. Gu, E. Marin, N. Sugano, G. Pezzotti, Mechanisms induced by transition metal contaminants and their effect on the hydrothermal stability of zirconia-containing bioceramics: an XPS study, Phys. Chem. Chem. Phys. 20 (2018) 28929–28940.
[30] Z. Zhou, X. Liu, Y. Hu, Z. Liao, S. Cheng, M. Xu, An efficient sorbent based on $CuCl_2$ loaded CeO_2-ZrO_2 for elemental mercury removal from chlorine-free flue gas, Fuel 216 (2018) 356–363.
[31] D.J. Morgan, Resolving ruthenium: XPS studies of common ruthenium materials, Surf. Interface Anal. 47 (2015) 1072–1079.
[32] F. Yu, C. Wang, H. Ma, M. Song, D. Li, Y. Li, S. Li, X. Zhang, Y. Liu, Revisiting Pt/TiO_2 photocatalysts for thermally assisted photocatalytic reduction of CO_2, Nanoscale 12 (2020) 7000–7010.
[33] C. Yang, C. Pei, R. Luo, S. Liu, Y. Wang, Z. Wang, Z.J. Zhao, J. Gong, Strong electronic oxide-support interaction over In_2O_3/ZrO_2 for highly selective CO_2 hydrogenation to methanol, J. Am. Chem. Soc. 142 (2020) 19523–19531.
[34] Z. Zhang, P. Li, Q. Wang, Q. Feng, Y. Tao, J. Xu, C. Jiang, X. Lu, J. Fan, M. Gu, H. Li, H. Wang, Mo modulation effect on the hydrogen binding energy of hexagonal-close-packed Ru for hydrogen evolution, J. Mater. Chem. A 7 (2019) 2780–2786.
[35] Y. Song, X. Cui, T. Deng, Z. Qin, W. Fan, Solvent effect on the activity of Ru-Co_3O_4 catalyst for liquid-phase hydrogenation of CO_2 into methane, J. Fuel Chem. Technol. 49 (2021) 178–185.
[36] B. Wu, X. Yu, M. Hunag, L. Zhoug, Y. Sun, Rh single atoms embedded in CeO_2 nanostructure boost CO_2 hydrogenation to HCOOH, Chin. J. Chem. Eng. 43 (2022) 192–204.
[37] E.M. Kock, M. Kogler, T. Bielz, B. Klotzer, S. Penner, In situ FT-IR spectroscopic study of CO_2 and CO adsorption on Y_2O_3, ZrO_2, and Yttria-stabilized ZrO_2, J. Phys. Chem. C 117 (2013) 17666–17673.
[38] J.A.H. Dreyer, P. Li, L. Zhang, G.K. Beh, R. Zhang, P.H.L. Sit, W.Y. Teoh, Influence of the oxide support reducibility on the CO_2 methanation over Ru-based catalysts, Appl. Catal. B Environ. 219 (2017) 715–726.
[39] J. Wang, G. Li, Z. Li, C. Tang, Z. Feng, H. An, H. Liu, T. Liu, C. Li, A highly selective and stable ZnO-ZrO_2 solid solution catalyst for CO_2 hydrogenation to methanol, Sci. Adv. 3 (2017), e1701290.
[40] K. Liu, X. Xu, J. Xu, X. Fang, L. Liu, X. Wang, The distributions of alkaline earth metal oxides and their promotional effects on Ni/CeO_2 for CO_2 methanation, J. CO2 Util. 38 (2020) 113–124.
[41] J. Xu, X. Su, H. Duan, B. Hou, Q. Lin, X. Liu, X. Pan, G. Pei, H. Geng, Y. Huang, T. Zhang, Influence of pretreatment temperature on catalytic performance of rutile TiO_2-supported ruthenium catalyst in CO_2 methanation, J. Catal. 333 (2016) 227–237.
[42] P. Panagiotopoulou, Hydrogenation of CO_2 over supported noble metal catalysts, Appl. Catal. A Gen. 542 (2017) 63–70.
[43] Y. Wang, J. Zhao, Y. Li, C. Wang, Selective photocatalytic CO_2 reduction to CH_4 over Pt/In_2O_3: Significant role of hydrogen adatom, Appl. Catal. B Environ. 226 (2018) 544–553.
[44] C. Asokan, H.V. Thang, G. Pacchioni, P. Christopher, Reductant composition influences the coordination of atomically dispersed Rh on anatase TiO_2, Catal. Sci. Technol. 10 (2020) 1597–1601.
[45] H.V. Thang, S. Tosoni, L. Fang, P. Bruijnincx, G. Pacchioni, Nature of sintering-resistant, single-atom Ru species dispersed on zirconia-based catalysts: a DFT and FTIR study of CO adsorption, ChemCatChem 10 (2018) 2634–2645.
[46] X. Xu, Y. Tong, J. Huang, J. Zhu, X. Fang, J. Xu, X. Wang, Insights into CO_2 methanation mechanism on cubic ZrO_2 supported Ni catalyst via a combination of experiments and DFT calculations, Fuel 283 (2021), 118867.
[47] A. Vasileff, X. Zhi, C. Xu, L. Ge, Y. Jiao, Y. Zheng, S. Qiao, Selectivity control for electrochemical CO_2 reduction by charge redistribution on the surface of copper alloys, ACS Catal. 9 (2019) 9411–9417.
[48] S. Akamaru, T. Shimazaki, M. Kubo, T. Abe, Density functional theory analysis of methanation reaction of CO_2 on Ru nanoparticle supported on TiO_2 (101), Appl. Catal. A Gen. 470 (2014) 405–411.
[49] L. Foppa, C. Coperet, A. Comas-Vives, Increased back-bonding explains step-edge reactivity and particle size effect for CO activation on Ru nanoparticles, J. Am. Chem. Soc. 138 (2016) 16655–16668.

[50] Y. Yan, Q. Wang, C. Jiang, Y. Yao, D. Lu, J. Zheng, Y. Dai, H. Wang, Y. Yang, Ru/Al_2O_3 catalyzed CO_2 hydrogenation: oxygen-exchange on metal-support interfaces, J. Catal. 367 (2018) 194–205.
[51] S. Chen, A.M. Abdel-Mageed, M. Li, S. Cisneros, J. Bansmann, J. Rabeah, A. Brückner, A. Groß, R.J. Behm, Electronic metal-support interactions and their promotional effect on CO_2 methanation on Ru/ZrO_2 catalysts, J. Catal. 400 (2021) 407–420.
[52] P. Dongapure, S. Bagchi, S. Mayadevi, R.N. Devi, Variations in activity of Ru/TiO_2 and Ru/Al_2O_3 catalysts for CO_2 hydrogenation: an investigation by in-situ infrared spectroscopy studies, Mol. Catal. 482 (2020), 110700.